Homology Modeling and Molecular Dynamics Simulations of Transmembrane Domain Structure of Human Neuronal Nicotinic Acetylcholine Receptor

Alexander C. Saladino,* Yan Xu,*† and Pei Tang*†

Departments of *Anesthesiology and †Pharmacology, University of Pittsburgh School of Medicine, Pittsburgh, Pennsylvania

ABSTRACT   A three-dimensional model of the transmembrane domain of a neuronal-type nicotinic acetylcholine receptor (nAChR), $(\alpha4)_2(\beta2)_3$, was constructed from a homology structure of the muscle-type nAChR recently determined by cryo-electron microscopy. The neuronal channel model was embedded in a fully hydrated DMPC lipid bilayer, and molecular-dynamics simulations were performed for 5 ns. A comparative analysis of the neuronal- versus muscle-type nAChR models revealed many conserved pore-lining residues, but an important difference was found near the periplasmic mouth of the pore. A flickering salt-bridge of $\alpha4$-E266 with its adjacent $\beta2$-K260 was observed in the neuronal-type channel during the course of the molecular-dynamics simulations. The narrowest region, with a pore radius of ~2 Å formed by the salt-bridges, does not seem to be the restriction site for a continuous water passage. Instead, two hydrophobic rings, formed by $\alpha4$-V259, $\alpha4$-L263, and the homologous residues in the β_2-subunits, act as the gates for water flow, even though the region has a slightly larger pore radius. The model offers new insight into the water transport across the $(\alpha4)_2(\beta2)_3$ nAChR channel, and may lead to a better understanding of the structures, dynamics, and functions of this family of ion channels.

INTRODUCTION

The nicotinic acetylcholine receptors (nAChRs) belong to a superfamily of Cys-loop receptors that are characterized by a pair of disulfide-bonded cysteines separated by 13 residues in the extracellular domain. Other members in the super-family include the 5-hydroxytryptamine type-3 receptors, the glycine receptors, and the γ-aminobutyric acid type A and type C (GABA$_A$ and GABA$_c$) receptors. It is believed that these receptors share a structural architecture and consist of five subunits in a pentameric arrangement. Each subunit of the receptors has an extended extracellular N-terminus, four transmembrane domains (TM1–TM4), and a short C-terminus. The TM2 domain from each subunit is assembled to form the pore of a channel (Karlin, 2002). The channel gating is controlled by the binding status of neurotransmitters in the extracellular domain, which propagates conformational change from the extracellular domain to the transmembrane domain and results in a transformation of the ion channel from one state to another. This conversion allows selected ions to pass the lipid bilayer through the ion channel upon agonist binding to the receptor. Although a significant body of knowledge has been accumulated toward the understanding of the channel gating, the structural and dynamical aspects of it remain to be elucidated.

There are multiple subtypes of nAChRs, each with a unique pharmacological profile and involvement in different phys-iological and behavioral processes. The muscle-type nAChRs from combinations of five different subunits ($\alpha1$, $\beta1$, δ, γ, or ε) have been found to mediate neuromuscular transmission at the skeletal neuromuscular junction. Neuronal-type nAChRs are much more diverse than their muscle counterparts. A wide range of neuronal nAChR subunits ($\alpha2-\alpha10$ and $\beta2-\beta4$) are capable of forming various subtype receptors that can intervene in fast synaptic transmission through the peripheral and central nervous system with different functional charac-teristics. In contrast to muscle-type receptors, most neuronal nAChR subunits assemble according to a general $(\alpha)_2(\beta)_3$ stoichiometry. The $\alpha7-\alpha9$ subunits, however, are known to form homopentamers. Among neuronal nAChR subtypes, $(\alpha4)_2(\beta2)_3$ has been identified as being the major central-nervous system constituent of the nicotinic receptors (McGehee and Role, 1995) that account for most of the high affinity binding sites in the brain for nicotine. Mutations in the TM2 domain of the $(\alpha4)_2(\beta2)_3$ subtype have been linked to certain forms of epilepsy (Itier and Bertrand, 2002). Moreover, the $(\alpha4)_2(\beta2)_3$ subtype is much more sensitive to inhibition by volatile anesthetics than the $\alpha7$ homomeric neuronal subtype or the muscle-type (Tassonyi et al., 2002). All of these facts make the $(\alpha4)_2(\beta2)_3$ subtype an interesting subject in the present study.

The structural information of neuronal nAChRs is currently lacking. The recent acquirement of a structure at the atomic resolution of 2.7 Å by x-ray crystallography (Brejc et al., 2001) for the acetylcholine binding protein, which shares a 20–25% sequence identity with the nAChR extracellular domain, greatly enhanced our knowledge about the extracel-lular domain structures of nAChRs. For transmembrane domains, high-resolution structures of TM2 domains from

various subunits in different receptors have been resolved using nuclear magnetic resonance (NMR), including the δ2-subunit of the nAChR (Opella et al., 1999), the β2-subunit of the nAChR (Yushmanov et al., 2003b), and the α1-subunit of the human glycine receptor (Tang et al., 2002; Yushmanov et al., 2003a). Recently, a structural model of the transmembrane domains of the muscle-type AChR from *Torpedo californica* has been derived from cryogenic electron microscopy (Miyazawa et al., 2003; Unwin, 2003). This model serves as a structure template for the homology modeling of the TM domains of the $(\alpha4)_2(\beta2)_3$ nAChRs in the present study. Homology modeling and the subsequent molecular dynamics (MD) simulations of the TM domains of $(\alpha4)_2(\beta2)_3$ nAChR in a fully hydrated 1,2-dimyristoyl-*sn*-glycero-3-phosphocholine (DMPC) bilayer revealed many molecular details that may further the understanding of this important and complex receptor.

METHODS

Homology modeling

The human nAChR α4 (P43681) (Monteggia et al., 1995; Steinlein et al., 1995) and β2 (P17787) (Anand and Lindstrom, 1990) sequences were obtained from the ExPASy Molecular Biology Server (http://us.expasy.org) (Gasteiger et al., 2003) and aligned with the *Torpedo californica* α1 (P02710) (Kao and Karlin, 1986; Noda et al., 1982) and β1 (P02712) (Noda et al., 1983; Raftery et al., 1980) sequences using CLUSTALW (http://www.ebi.ac.uk/clustalw) (Thompson et al., 1994). The TM domain structures of α4 and β2 were generated from the sequence alignment and the structural template for the TM domains of the *Torpedo californica* nAChR (PDB ID 1OED) (Unwin, 2003), using the MODELLER program (http://salilab.org/modeller) (Fiser et al., 2000). The electrocyte muscle-type nAChR is composed of two α1- and one β1-, δ-, and γ-subunits, whereas the $(\alpha4)_2(\beta2)_3$ nAChR consists of two α4- and three β2-subunits in the configuration of $(\alpha4)(\beta2)(\alpha4)(\beta2)(\beta2)$ (Anand et al., 1991). Two α4-subunits and one of the β2-subunits were directly modeled on the basis of homology to the muscle-type α1- and the β1-subunits, respectively. The structures of the other two β2 were first modeled against the muscle β1-subunit and then aligned to the δ- and γ-subunits using VMD (http://www.ks.uiuc.edu/research/vmd) (Humphrey et al., 1996). The resulting model was energy-minimized with NAMD 2.5 (http://www.ks.uiuc.edu/Research/namd) (Kale et al., 1999) using a conjugate gradient and line-search algorithm (Polak, 1971) for 10 ps with a 500 kcal/mol/Å^2 harmonic restraint on the backbone of the protein. The intracellular loop connecting the TM3 and the TM4 was omitted in the target model because of its absence in the original template.

System preparations

The lipid patch for the system was built from a pre-equilibrated and fully hydrated ($n_{\text{w}} = 29.2$) DMPC bilayer (Tang and Xu, 2002; Zubrzycki et al., 2000) by enlarging the original 200-lipid-molecule patch to a 369-lipid-molecule patch to accommodate the size of the $(\alpha4)_2(\beta2)_3$ nAChR. This enlarged DMPC bilayer system ($110 \times 110 \times 60$ Å^3) was further simulated under a constant pressure of 1 atm and a constant temperature of 303 K for 1 ns before the energy-minimized TM domains of the $(\alpha4)_2(\beta2)_3$ nAChR was embedded into it. Although a novel preparation protocol (Allen et al., 2003; Woolf and Roux, 1996) has been reported for the initial placement of a small number of lipid molecules around channel proteins, a more traditional approach was taken in the present study because of the need for a much larger membrane patch. Starting with a pre-equilibrated DMPC membrane,

$\sim$65 lipid molecules were removed from each layer of the bilayer to generate enough spaces for the insertion of the channel. The channel axis was set parallel to the membrane normal. The water molecules within 0.8 Å of the protein were also removed. A single file of TIP3 water was inserted through the channel. A sodium ion was introduced into the system to reach overall electrical neutrality. The resulting system had 239 DMPC lipids, 10,388 waters, one sodium ion, and one TM pentamer of the $(\alpha4)_2(\beta2)_3$ nAChR, for a total of 69,650 atoms. Before MD simulations, the system was energy-minimized using a conjugate gradient and line-search algorithm for 10 ps and equilibrated for 100 ps under constant volume and constant temperature (303 K) conditions. A harmonic restraint of 500 kcal/mol/Å^2 was applied to the backbone atoms of the protein during the system equilibration.

Molecular dynamics simulations

Molecular dynamics simulations were performed using NAMD 2.5 at the Pittsburgh Supercomputer Center on either the Cray T3E or the HP Alpha Server GS1280 parallel supercomputers. The bonded interactions were calculated at every time-step, the short-range nonbonded interactions at every two time-steps, and the long-range electrostatics interactions at every four time-steps. The pair-list of the nonbonded interaction was recalculated every 20 time-steps with a pair-list distance of 11.5 Å. The short-range nonbonded interactions were defined as van der Waals and electrostatics interactions between particles within 10 Å. A smoothing function was employed for the van der Waals interactions at a distance of 8.5 Å. The long-range electrostatic forces were calculated with the particle-mesh Ewald (Darden et al., 1993). CHARMM27 (MacKerell et al., 1998) force-field parameters were used in all simulations in this study. Periodic boundary conditions and water wrapping were activated in the simulations. The SHAKE routine with a tolerance of 10^{-5} Å was used in all simulations.

The equilibrated system was simulated for 1 ns with a 500 kcal/mol/Å^2 restraint on the protein backbone under 1 atm constant pressure and 303 K constant temperature (NPT) using the Nosé-Hoover Langevin piston pressure control (Hoover, 1985; Nose, 1984) and the Langevin damping dynamics (Brünger, 1992), respectively. The interface between lipids and the protein was greatly improved after the first 1-ns NPT simulation. The constraint on the backbone of the protein was gradually reduced to zero in the subsequent 1-ns NPT simulations to further equilibrate the entire protein-lipid system without causing any destabilization of the protein backbone. After the backbone constraint was completely released, NPT simulations were carried out for addition 3 ns, resulting in a total of 5-ns simulations. The time-steps were 1 fs for the initial 3-ns and 2 fs for the rest 2-ns simulations. The atomic coordinates and velocities were saved every 1000 time-steps, and coordinate trajectories were saved every 500 time-steps for subsequent data analysis. It took approximately five days to achieve 1-ns simulation for the system using eight 1.15-GHz EV7 processors on the HP Alpha Server GS1280 supercomputer at the Pittsburgh Supercomputer Center.

Data process and analysis

The HOLE program, in conjunction with auxiliary routines (http://www.bip.bham.ac.uk/hole/) (Smart et al., 1993), was used to calculate the pore radius. VMD, with home-developed scripts, was used for system visualizations and all other analysis. The root mean-square deviations (RMSD) and the root mean-square fluctuations (RMSF) were calculated for each subunit.

RESULTS AND DISCUSSION

Sequence alignment and homology modeling

Because of an overall $\sim$60% sequence identity between the template and the target, as illustrated in Fig. 1, the modeling
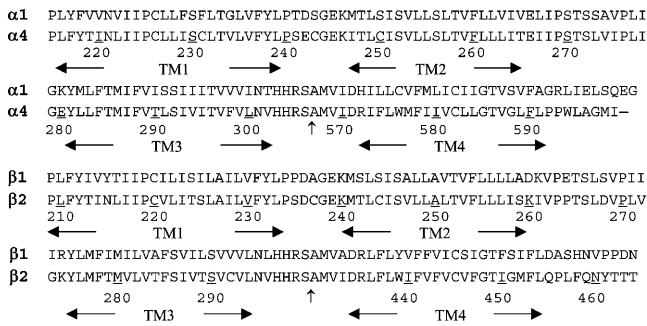
```
α1   PLYFVVNVIIPCLLFSFLTGLVFYLPTDSGEKMTLSISVLLSLTVFLLVIVELIPSTSSAVPLI
α4   PLFYTINLIIPCLLISCLTVLVFYLPSECGEKITLCISVLLSLTVFLLLITEIIPSTSLVIPLI
        220       230       240       250       260       270
      ←———— TM1 ————→              ←———— TM2 ————→

α1   GKYMLFTMIFVISSIIITVVVINTHHRSAMVIDHILLCVFMLICIIGTVSVFAGRLIELSQEG
α4   GEYLLFTMIFVTLSIVITVFVLNVHHRSAMVIDRIFLWMFIIVCLLGTVGLFLPPWLAGMI-
        280       290       300    ↑ 570      580       590
      ←———— TM3 ————→              ←———— TM4 ————→

β1   PLFYIVYTIIPCILISILAILVFYLPPDAGEKMSLSISALLAVTVFLLLLADKVPETSLSVPII
β2   PLFYTINLIIPCVLITSLAILVFYLPSDCGEKMTLCISVLLALTVFLLLISKIVPPTSLDVPLV
        210       220       230       240       250       260       270
      ←———— TM1 ————→              ←———— TM2 ————→

β1   IRYLMFIMILVAFSVILSVVVLNLHHRSAMVADRLFLYVFFVICSIGTFSIFLDASHNVPPDN
β2   GKYLMFTMVLVTFSIVTSVCVLNVHHRSAMVIDRLFLWIFVFVCVFGTIGMFLQPLFQNYTTT
          280       290       ↑          440       450       460
      ←———— TM3 ————→              ←———— TM4 ————→
```

FIGURE 1 The sequence of the human α4 (*top*) and β2 (*bottom*) are aligned with the *Torpedo californica* α1 and the β1, respectively. The numbering corresponds to the sequences of α4 and β2. The sequence break points between the TM3 and the TM4 domains in the structure of 1OED are indicated by the vertical arrows (↑).

of the TM domains of the $(\alpha 4)_2 (\beta 2)_3$ nAChR from the structure of *Torpedo californica* nAChR (Miyazawa et al., 2003; Unwin, 2003) was rather straightforward. Among four transmembrane domains, TM2 domains have the most conserved residues (75–80%), whereas TM4 domains have the least (50–55%). The loops connecting TM1 and TM2 and the loops connecting TM2 and TM3 have sequence identities of 57% and 53%, respectively. As expected, the target model did not exhibit major differences from the template when they were superimposed. The high percentage of sequence identity ensured the quality of the homology model, but the accuracy of the target is limited to the relatively low resolution (~4 Å) inherent to the template. Nevertheless, the homology model with further MD simulations in a fully hydrated lipid bilayer is useful for identifying the relevant structural and dynamical information before a high-resolution experimental structure becomes available.

Ideally, one would hope to run several parallel simulations with slightly different starting models as controls to determine whether the control simulations will yield results converging to those reported here. This exercise, however, would be forbiddingly expensive in terms of computing cost. Fortunately for our study, the target protein has an extremely high sequence identity to the template so that structural variation of the starting proteins derived from the homology modeling was not significant. Therefore, omitting the control simulations will not greatly change the major conclusions of the current study.

Stability and flexibility of the channel

To explore the intrinsic dynamics and the structural stability of the TM domains of the $(\alpha 4)_2 (\beta 2)_3$ nAChR channel, the initially applied harmonic restraints on the backbone of the protein were gradually released during the course of the second 1-ns simulation. Fig. 2 shows the top view of the $(\alpha 4)_2 (\beta 2)_3$ nAChR channel and the side views of the system after additional 1.5-ns MD simulations without any
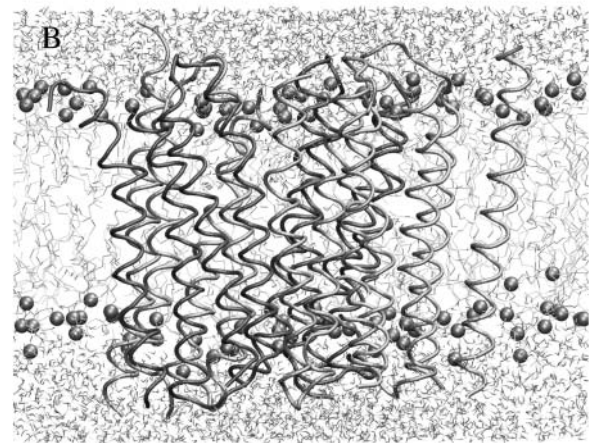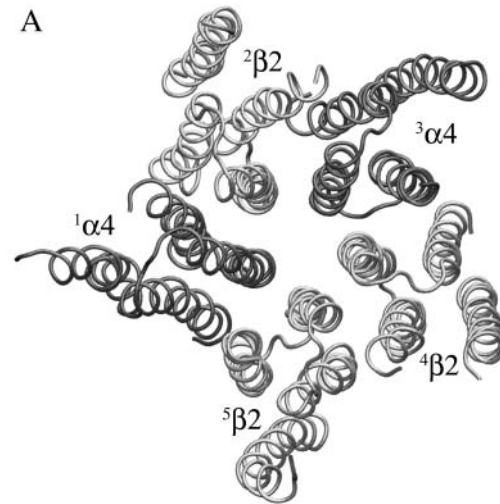
FIGURE 2 (*A*) A top view and (*B*) side view of the TM domain model of $(\alpha 4)_2 (\beta 2)_3$ nAChR embedded in a fully hydrated DMPC lipid bilayer after 3.61-ns simulations.

restraints, indicating that the pentameric topology of the channel was well maintained under the condition of no restraints.

The overall stability of the channel was evaluated using the Cα RMSD of the TM segments and is illustrated in Fig. 3 *A*. Stepwise rising of RMSD correlates well with the gradual release of the harmonic restraints on the backbone residues, reaching a value of ~1.5 Å at the point of the complete removal of the backbone restraints. A plateau of ~2.4 Å RMSD was achieved within 1 ns of unrestrained simulation, suggesting that a 3-ns unrestrained simulation was sufficient for stabilizing a fully relaxed channel model. An average of ~2.4 Å drift from the initial model structure is reasonably low in comparison to those from similar simulations of ion channel proteins (Arinaminpathy et al., 2003; Berneche and Roux, 2000; Gullingsrud et al., 2001; Shrivastava and Sansom, 2000; Tieleman and Berendsen, 1998). The small deviation from the initial model was partially reflected in the reorientation of the helices. Fig. 3 *B* shows that transmembrane helices underwent certain changes in their
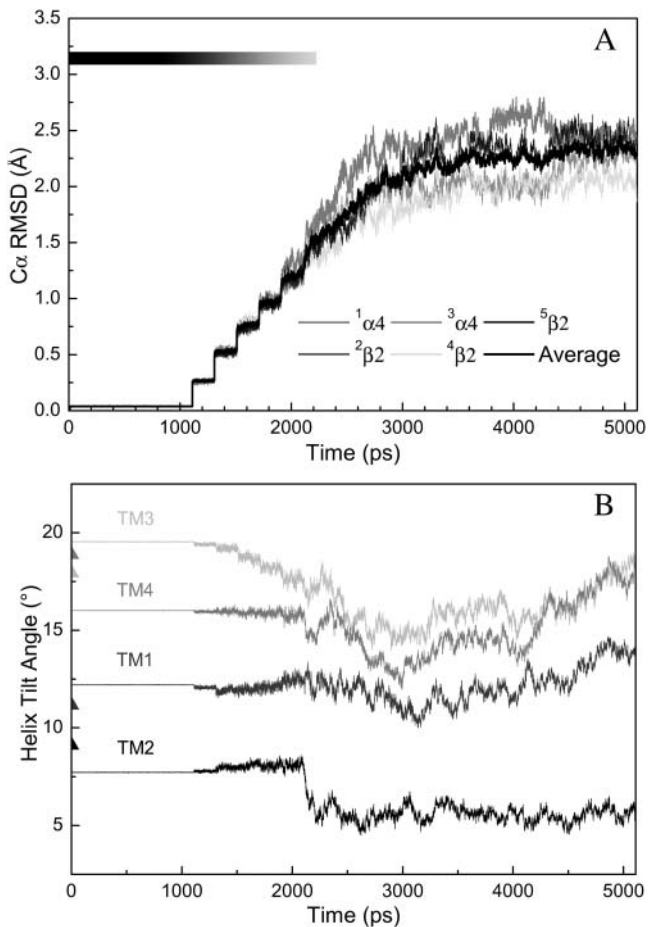
FIGURE 3 (*A*) Structural drift revealed as RMSDs of all Cα atoms in the helical regions of each subunit. The grayscale on the top left of the figure reflects the strength of applied harmonic restraint forces to the backbone of the protein. Stepwise jumps of RMSDs correlate to a gradual reduction of harmonic restraints. A complete relief of restraints at 2.11 ns led to smooth increases of RMSD, which reached a plateau ∼3 ns. (*B*) Averaged helical tilt angles relative to the bilayer norm (*z* axis) as a function of MD simulation time. The course of applied harmonic restraints was identical to that in *A*.

FIGURE 4 Structural flexibility shown as RMSFs of all Cα atoms averaged over all subunits from the last 3-ns of unrestrained simulations.

orientations relative to the bilayer normal (*z* axis) during the simulation, but at the end of 5-ns simulation none of the TM domains had more than a 5° change in their tilt angles. The fluctuations of the helix-tilt angles in the current system are apparently smaller than what was previously reported in an isolated TM2δ₅ system (Law et al., 2003), where the helix-tilt angles fluctuated over a range of ∼5°–25° on a timescale of ∼2–5 ns.

The channel flexibility was assessed by Cα RMSFs that were averaged over the last 2-ns simulations and across all five subunits. Typical RMSF patterns, with low RMSF values for the well-structured TM helical regions and high values for the loosely-structured loop regions or domain termini, are shown in Fig. 4. The profound increase in RMSF values at both termini of TM4 was presumably due to the disconnection of TM4 from the other three domains. Most TM helical regions experience ∼1 Å fluctuation, but TM2
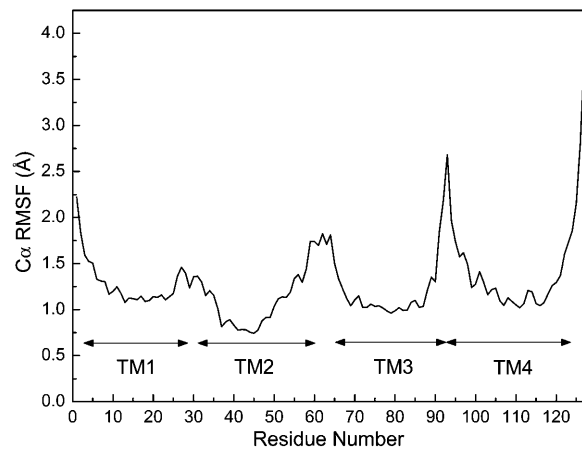
has a slightly lower RMSF that concurs with the observation on the TM2δ₅ system (Law et al., 2003).

Protein-lipid interactions

Ionic or hydrophobic interactions have been traditionally considered as the predominate interactions between the protein and the lipid. The interactions of muscle-type nAChR with the lipid bilayer were previously identified using hydrophobic photoreactive probes (Blanton and Cohen, 1992, 1994; Blanton et al., 1998). The photolabeling pattern indicated that the TM4 had a broad face to membrane lipids; the TM1 and the TM3 also had a few residues in contact with the lipid. The homologs of these lipid-exposing residues have been examined carefully in the current (α4)₂(β2)₃ model. They are in good agreement with the experimental results. Most of these lipid-exposing residues interact with lipid through hydrophobic interactions.

In addition to the predominate hydrophobic interactions, the interactions between the belts of amphipathic aromatic side chains on the surface of the protein and the interfacial regions of the bilayer have drawn much attention lately (Domene et al., 2003; White and Wimley, 1998). These Trp- and Tyr-constituted belts may facilitate the anchoring of the protein within the membrane through their interactions with the polar headgroups of the membrane lipids. Attention has been paid to the same in the current model. As demonstrated in Fig. 5, the interactions between lipid headgroups and the belts of Tyr side chains are present in the cytoplasmic end of the TM1 and the periplasmic end of the TM3. The Trp and Tyr residues on both termini of the TM4 have profound interactions with the lipids, as evidenced by the two distinct bands in Fig. 5. The intensity of the bands directly reflects how many atoms of the lipid headgroup are within 3.5 Å of a Trp or a Tyr. It is clear that the aromatic belts on the TM4 carry stronger interactions with lipid than those on the TM1
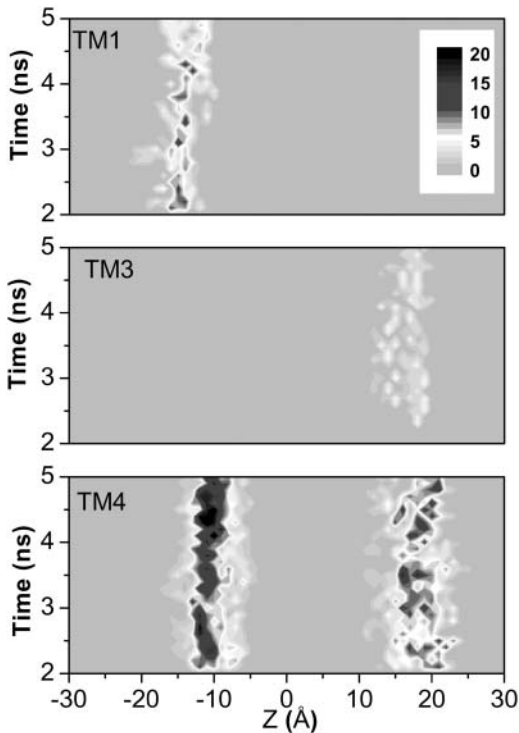
FIGURE 5   Interactions (≤ 3.5 Å) of tryptophan (in TM4) or tyrosine (in TM1, TM3, and TM4) with DMPC lipid headgroups. The number of atoms involved in the interactions is shown as a function of position along the bilayer normal (Z) and simulation time.

and the TM3. This observation seems to be consistent with the speculation that TM4 is the outermost transmembrane domain (Bouzat et al., 2000) and may involve less in conformation changes during the channel gating (Unwin et al., 2002).

Protein-protein interactions

Similar to the interactions between protein and lipids, hydrophobic and ionic interactions contribute to helix-helix packing and ultimately to the stability of a protein. In the current model, we found that Leu dominates 25% of total helical-helical interactions through close contact (<2.8 Å) with another Leu or with residues Ile, Phe, Val, Thr, and Ser. Within a subunit, helical-helical interactions are moderately uniform among the four domains: TM1 26.3%, TM2 25.4%, TM3 29%, and TM4 19.3%. Among six possible combinations of the interactions, TM1–TM2 comprises the most ($\sim 28.3\%$ of the total number of contacts) and TM2–TM4 the least (0.3%); the rest of them are in the order of TM3–TM4 ($\sim 25\%$), TM2–TM3 ($\sim 22\%$), TM1–TM4 (13.4%), and TM1–TM3 (10.9%). The distribution of helical interactions between subunits is distinctly different from that within a subunit. TM4 has no cross-subunit interactions. The percentages of intersubunit interactions are distributed among TM1, TM2, and TM3 as 32%, 47%, and 21% of

the total number of contacts, respectively. Of all helical-helical interactions, 56% belong to hydrophobic interactions, 37% to nonpolar-polar interactions, and 7% to polar-polar interactions.

The pore-lining residues in the current model are consistent with the previous experimental findings, either using cysteine mutagenesis (Yamakura et al., 2000) or using the substituted-cysteine accessibility method (Wilson and Karlin, 2001). Because of the high percentage of sequence identity in the TM2 domain of the $(\alpha 4)_2 (\beta 2)_3$ and the muscle-type nAChR (Miyazawa et al., 2003), it is anticipated that the models share many identical pore residues. One of the exceptions in the $(\alpha 4)_2 (\beta 2)_3$ model, however, is the Lys[260] near the C-termini of TM2 domains of three $\beta 2$-subunits, a replacement of the Asp[268] in a homologous position of the $\beta 1$-subunit. Consequently, the conserved $\alpha 4$-Glu[266] forms alternate salt-bridges with Lys[260] in the adjacent $\beta 2$-subunits, as shown in Fig. 6. The salt-bridge was not present in the initial model but formed after $\sim$2-ns simulations. It was noticed that individual salt-bridges could last for several nanoseconds, and sometimes two salt-bridges could form simultaneously. This type of intersubunit salt-bridge may facilitate the stability of the channel quaternary structure. Frequent alternation in the salt-bridge partners reflects the highly dynamic nature of the periplasmic mouth of the channel. A detailed analysis of the simulation trajectories indicated that the formation of a salt-bridge resulted in a smaller pore radius (~ 2.1 Å), which could be reduced even further (~ 1.3 Å) if two salt-bridges were formed simultaneously.

Is the salt-bridge girdle critical to the opening and closing of the channel? Previous studies on gating mechanisms of the OmpA channel suggested that the channel's open or
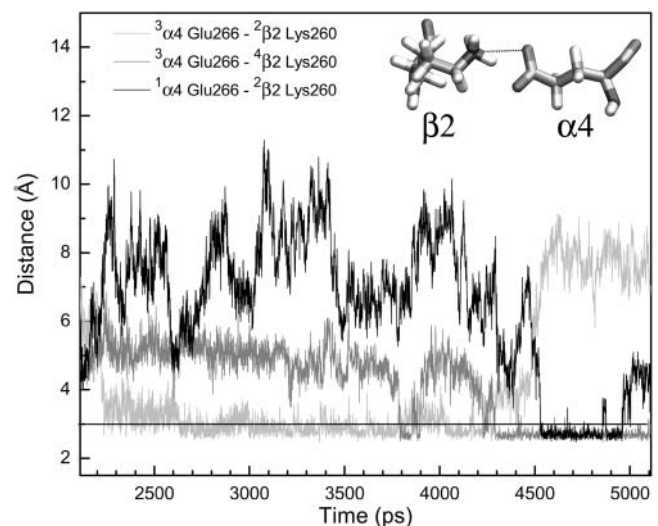

FIGURE 6   Salt-bridges between $\alpha 4$ and $\beta 2$. The distances from the carboxylate oxygen of $\alpha 4$-Glu[266] to an adjacent side-chain amine of $\beta 2$-Lys[260] (see *inset*) are plotted as a function of simulation time.

closed states could be almost synchronized with the formation of alternate salt-bridges in the pore between Arg[138] with either Glu[52] (closed state) or Glu[128] (open state) (Bond et al., 2002). In the case of nAChR, α4- Glu[266] is conserved for all α-subtypes, and β2-Lys[260] has an analogous lysine in the β4-subunit (β4-Lys[262]). Thus, any neuronal-type nAChR involving α and β2 or β4 may form a salt-bridge between the α- and β-subunits near the extracellular entrance of the channel pore. It is unlikely, however, that the salt-bridges in the $(\alpha4)_2(\beta2)_3$ nAChR channel play any significant role as a gate, because during the entire 5-ns simulation, the continuity of the water passage, as judged by the water cluster density, was never constricted near these salt-bridges.

Pore and water profiles

The profiles of pore radius and water distribution along the channel are valuable information for assessing a possible gate. It is assumed that disruption of the water passage in the channel reflects the obstruction to the ion movement along the channel. Understandably, water occupancy in the channel is a necessary, but not sufficient, condition for ion occupancy inside the channel. Nevertheless, it is reasonable to consider that a water-restricting region in the channel might also be a gate for ions to pass through. Fig. 7 shows three snapshots of possible profiles of pore radius in relation to the water distribution at the selected simulation time-points. The originally docked single file of water inside the channel was completely disrupted after a very brief
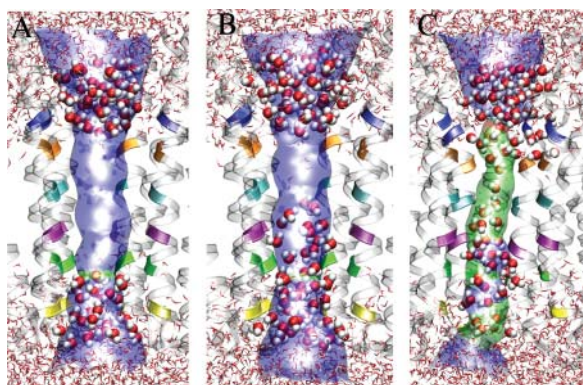

FIGURE 7 Snapshots of the pore profiles and the water passage through the pore. For clarity, only part of the protein backbone and water in or close to the pore are shown. (The pore-lining residues are color-coded: *yellow*, α4-Thr[248] and β2-Thr[242]; *green*, α4-Ser[252] and β2-Ser[246]; *purple*, α4-Leu[255] and β2-Leu[249]; *cyan*, α4-Val[259] and β2-Val[253]; *orange*, α4-Leu[263] and β2-Leu[257]; and *blue*, α4-Glu[266] and β2-Lys[260].) The pore profile was generated using (the) HOLE. (The color codes for the pore radius: *red*, <2.0 Å; *green*, between 2.0 Å and 3.0 Å; and *blue*, >3.0 Å.) (*A*) A water vacuum is formed after 546 ps of simulation. (*B*) A water vacuum is reduced to between residues α4-Val[259] and α4-Leu[263] after 1110 ps of simulation. (*C*) A continuous water passage is formed after 4110 ps of simulation. A single file of water flows through the hydrophobic rings at α4-Val[259] and α4-Leu[263].

restrained simulation ($\sim$90 ps). Consequently, a region devoid of water was generated in the channel, as shown in Fig. 7 *A*. This region is bordered by the pore-lining residues Ser[251], Leu[255], Val[259], and Leu[263] of the α4, and their homologous residues Ser[246], Leu[249], Val[253], and Leu[257] of the β2. Ser[251] of the α4 and Ser[246] of the β2 defined the narrowest pore radius ($\leq$3 Å), which is similar to that in the muscle-type nAChR. In the subsequent $\sim$500-ps restrained simulation, water molecules burst through the serine ring (α4-Ser[251] and β2-Ser[246]) and further through the leucine ring (α4-Leu[255] and β2-Leu[249]), whereas the pore-radius changed insignificantly, as depicted in Fig. 7 *B*. It took a much longer simulation time ($\sim$2.5 ns) to let a continuous file of water fill the region bounded by Val[259] and Leu[263] of the α4 and Val[253] and Leu[257] of the β_2. The continuity of this file of water subsisted for a substantial amount of time, with occasional interruption, in the remaining simulations. The simulation results seem to imply that residues α4-Val[259], α4-Leu[263], and their analogous β_2-Val[253], β_2-Leu[257] play a critical role in controlling and disrupting the continuity of water in the channel; they may also serve as a hydrophobic gate to ion permeations.

A water-restricting region is anticipated in the current channel model because its homology template is in a closed state (Miyazawa et al., 2003). In the model of the muscle-type nAChR, a hydrophobic girdle, contributed mainly by the side chains of α1-Leu[251], α1-Val[255], and their analogs in other subunits, was believed to provide an energetic barrier for the path of ion conductance. The girdle is identified as the gate of the pore of the muscle-type nAChR. In our model of the neuronal $(\alpha4)_2(\beta2)_3$ nAChR, however, the hydrophobic girdle seems to be shifted one pore-lining residue toward the C-terminus of TM2. This difference might result from the electrostatic interaction near the extracellular entrance of the channel. The existence of salt-bridges between α4-Glu[266] and β2-Lys[260] in the current model could make the pore entrance tighter at the interface of the membrane and extracellular water. Such salt-bridges, however, do not exist along the pore of the muscle-type nAChR. Further investigation maybe needed to confirm if the location of the hydrophobic girdle is affected by the formation of the salt-bridges one helical-turn away from the girdle.

The profiles of the pore radii and water distributions found in the present study also suggest that the restriction site to water passage does not necessarily coincide with the narrowest radius ($\sim$2 Å) defined by the polar side chains in the pore. Instead, region with slightly larger radius (2–3 Å) but with hydrophobic side chains can act as the true occlusion site. In essence, the energy barrier and geometric restriction to water transport can be physically separated, and they do not necessarily locate at the same place inside a channel. This finding has profound implications in defining the gate of a channel to ion transport. A geometric restriction should not be automatically translated as a functional gate.

Our finding that the true water barrier is located near the hydrophobic girdle correlates well with the gating models of muscle-type nAChR (Miyazawa et al., 2003) and K channels (Jiang et al., 2002). There is a discrepancy of ~1 Å between our simulated radius (2.3 Å) at the hydrophobic gate and the radius (3.1 Å) at the corresponding location inside the muscle-type model (Miyazawa et al., 2003). Before a higher resolution experimental structure becomes available for the nAChR, it is difficult to determine which value is more accurate. The reported pore radius of ~3.1 Å for nAChR seems much larger than the pore radii of several other closed ion channels whose high-resolution structures are currently available (Chang et al., 1998; Doyle et al., 1998; Kuo et al., 2003).

CONCLUSIONS

Homology modeling, combining with MD simulations, has been used successfully for many biological macromolecules, including the extracellular domain of the nAChR (Le Novere et al., 2002). The present study is the first attempt to explore the structures and dynamics of the complete TM domains of neuronal nAChR in an explicit membrane preparation. The modeled TM domain structure of human neuronal $(\alpha4)_2(\beta2)_3$ nAChR in DMPC lipid bilayers achieved reasonable convergence over the course of ~5-ns MD simulations. Longer simulation time will allow the acquisition of more trajectories and may better sample the dynamic properties, but it is computationally costly and very unlikely to have further impact on the structure. The helix-helix interactions between subunits or within a subunit, either through hydrophobic or ionic interactions, contribute to the stabilization of the channel structure. Aromatic belts constituted by Trp or Tyr residues are found in all TM domains except TM2. They may facilitate the stabilization of the channel structure in the membrane through their interaction with either periplasmic or cytoplasmic headgroups of the lipid membrane. The same type of interactions has also been identified in previous simulations with other ion channels (Domene et al., 2003; White and Wimley, 1998). It is highly possible that these aromatic belts exist in ion channel proteins in general to serve as the channel-anchoring force.

The salt-bridges near the periplasmic pore mouth between the TM2 of the $\alpha4$- and the $\beta2$-subunits are present in our homology model of the neuronal nAChR, but not in the muscle-type nAChR. Formation of the salt-bridges might have contributed to the reduction of the periplasmic pore radius, and consequently shifted the hydrophobic gate more toward periplasmic entrance of the channel. It is highly likely that the salt brides revealed in our model also exist in other heterosubunit neuronal nAChR, where the $\beta2$ or the $\beta4$ are involved, because both the $\beta2$ and $\beta4$ have Lys in the homologous positions to $\alpha4$-Glu[266]. The important finding of this study offers a clue for devising necessary experiments to assess the roles of the salt-bridges in the function of related neuronal nAChR.

The profiles of pore radius and water distribution along the channel during the course of simulations are well resolved in the present study. The fact that the water passage in the channel is restricted not by the narrowest pore region with polar residues but by a region with hydrophobic amino acid residues has important implications for the underlying principle of ion conductance. The hydrophobic nature of the restriction site in the present model supports the notion that a hydrophobic gate exists in nAChR and possibly in other members of the Cys-loop ion channel family. More extensive MD simulations on the current model can provide useful information regarding more challenge questions such as whether a closed gate in a narrow hydrophobic region can be opened by either a small increase (~1 Å) in pore radius or an increase in polarity (Beckstein et al., 2003).

As demonstrated in a recent study (Law and Sansom, 2004), an intermediate resolution structure derived from electron microscopy shows less stability in MD simulations than a homology model started from the high-resolution x-ray structure. The quality of initial structures is one of the determinants of the quality of the simulation results. High-resolution structures of several ion channels, including members of the K^+ channel (Doyle et al., 1998; Jiang et al., 2002, 2003; Kuo et al., 2003; Zhou et al., 2001), the mechanosensitive channel (Chang et al., 1998), and the Aquaporin family (Fu et al., 2000; Savage et al., 2003; Sui et al., 2001), have been solved in recent years. The availability of a high-resolution structure of the TM domain of Cys-loop receptor is urgently needed. We strongly believe that a combination of large-scale MD simulations, as presented in this study, and experimental approaches to yield high-resolution tertiary and quaternary structural constraints will reveal many other interesting properties of the Cys-loop receptor family.

REFERENCES

Allen, T. W., O. S. Andersen, and B. Roux. 2003. Structure of gramicidin a in a lipid bilayer environment determined using molecular dynamics simulations and solid-state NMR data. *J. Am. Chem. Soc.* 125:9868–9877.

Anand, R., W. G. Conroy, R. Schoepfer, P. Whiting, and J. Lindstrom. 1991. Neuronal nicotinic acetylcholine receptors expressed in *Xenopus* oocytes have a pentameric quaternary structure. *J. Biol. Chem.* 266:11192–11198.

Anand, R., and J. Lindstrom. 1990. Nucleotide sequence of the human nicotinic acetylcholine receptor $\beta2$ subunit gene. *Nucleic Acids Res.* 18:4272.

Arinaminpathy, Y., P. C. Biggin, I. H. Shrivastava, and M. S. Sansom. 2003. A prokaryotic glutamate receptor: homology modelling and molecular dynamics simulations of GluR0. *FEBS Lett.* 553:321–327.

Beckstein, O., P. C. Biggin, P. Bond, J. N. Bright, C. Domene, A. Grottesi, J. Holyoake, and M. S. Sansom. 2003. Ion channel gating: insights via molecular simulations. *FEBS Lett.* 555:85–90.

Berneche, S., and B. Roux. 2000. Molecular dynamics of the KcsA K$^+$ channel in a bilayer membrane. *Biophys. J.* 78:2900–2917.

Blanton, M. P., and J. B. Cohen. 1992. Mapping the lipid-exposed regions in the *Torpedo californica* nicotinic acetylcholine-receptor. *Biochemistry.* 31:3738–3750.

Blanton, M. P., and J. B. Cohen. 1994. Identifying the lipid-protein interface of the *Torpedo* nicotinic acetylcholine-receptor—secondary structure implications. *Biochemistry.* 33:2859–2872.

Blanton, M. P., L. J. Dangott, S. K. Raja, A. K. Lala, and J. B. Cohen. 1998. Probing the structure of the nicotinic acetylcholine receptor ion channel with the uncharged photoactivatable compound–3H-diazofluorene. *J. Biol. Chem.* 273:8659–8668.

Bond, P. J., J. D. Faraldo-Gomez, and M. S. Sansom. 2002. OmpA: a pore or not a pore? Simulation and modeling studies. *Biophys. J.* 83:763–775.

Bouzat, C., F. Barrantes, and S. Sine. 2000. Nicotinic receptor fourth transmembrane domain: hydrogen bonding by conserved threonine contributes to channel gating kinetics. *J. Gen. Physiol.* 115:663–672.

Brejc, K., W. J. van Dijk, R. V. Klaassen, M. Schuurmans, J. van Der Oost, A. B. Smit, and T. K. Sixma. 2001. Crystal structure of an ACh-binding protein reveals the ligand-binding domain of nicotinic receptors. *Nature.* 411:269–276.

Brünger, A. 1992. X-PLOR, Version 3.1: A System for X-Ray Crystallography and NMR. Yale University, New Haven, CT.

Chang, G., R. H. Spencer, A. T. Lee, M. T. Barclay, and D. C. Rees. 1998. Structure of the MscL homolog from *Mycobacterium tuberculosis*: a gated mechanosensitive ion channel. *Science.* 282:2220–2226.

Darden, T., D. York, and L. Pedersen. 1993. Particle-mesh Ewald—an $n \cdot \log(n)$ method for Ewald sums in large systems. *J. Chem. Phys.* 98:10089–10092.

Domene, C., P. J. Bond, S. S. Deol, and M. S. Sansom. 2003. Lipid/protein interactions and the membrane/water interfacial region. *J. Am. Chem. Soc.* 125:14966–14967.

Doyle, D. A., J. Morais Cabral, R. A. Pfuetzner, A. Kuo, J. M. Gulbis, S. L. Cohen, B. T. Chait, and R. MacKinnon. 1998. The structure of the potassium channel: molecular basis of K$^+$ conduction and selectivity. *Science.* 280:69–77.

Fiser, A., R. K. Do, and A. Sali. 2000. Modeling of loops in protein structures. *Protein Sci.* 9:1753–1773.

Fu, D., A. Libson, L. J. Miercke, C. Weitzman, P. Nollert, J. Krucinski, and R. M. Stroud. 2000. Structure of a glycerol-conducting channel and the basis for its selectivity. *Science.* 290:481–486.

Gasteiger, E., A. Gattiker, C. Hoogland, I. Ivanyi, R. D. Appel, and A. Bairoch. 2003. ExPASy: the proteomics server for in-depth protein knowledge and analysis. *Nucleic Acids Res.* 31:3784–3788.

Gullingsrud, J., D. Kosztin, and K. Schulten. 2001. Structural determinants of MscL gating studied by molecular dynamics simulations. *Biophys. J.* 80:2074–2081.

Hoover, W. G. 1985. Canonical dynamics: equilibrium phase-space distributions. *Phys. Rev. A.* 31:1695–1697.

Humphrey, W., A. Dalke, and K. Schulten. 1996. VMD: visual molecular dynamics. *J. Mol. Graphics.* 14:27–38.

Itier, V., and D. Bertrand. 2002. Mutations of the neuronal nicotinic acetylcholine receptors and their association with ADNFLE. *Neurophysiol. Clin.* 32:99–107.

Jiang, Y., A. Lee, J. Chen, M. Cadene, B. T. Chait, and R. MacKinnon. 2002. Crystal structure and mechanism of a calcium-gated potassium channel. *Nature.* 417:515–522.

Jiang, Y., A. Lee, J. Chen, V. Ruta, M. Cadene, B. T. Chait, and R. MacKinnon. 2003. X-ray structure of a voltage-dependent K$^+$ channel. *Nature.* 423:33–41.

Kale, L., R. Skeel, M. Bhandarkar, R. Brunner, A. Gursoy, N. Krawetz, J. Phillips, A. Shinozaki, K. Varadarajan, and K. Schulten. 1999. NAMD2: greater scalability for parallel molecular dynamics. *J. Comput. Phys.* 151:283–312.

Kao, P. N., and A. Karlin. 1986. Acetylcholine receptor binding site contains a disulfide cross-link between adjacent half-cystinyl residues. *J. Biol. Chem.* 261:8085–8088.

Karlin, A. 2002. Emerging structure of the nicotinic acetylcholine receptors. *Nat. Rev. Neurosci.* 3:102–114.

Kuo, A., J. M. Gulbis, J. F. Antcliff, T. Rahman, E. D. Lowe, J. Zimmer, J. Cuthbertson, F. M. Ashcroft, T. Ezaki, and D. A. Doyle. 2003. Crystal structure of the potassium channel KirBac1.1 in the closed state. *Science.* 300:1922–1926.

Law, R. J., and M. S. Sansom. 2004. Homology modelling and molecular dynamics simulations: comparative studies of human aquaporin-1. *Eur. Biophys. J.* 33:477–489.

Law, R. J., D. P. Tieleman, and M. S. Sansom. 2003. Pores formed by the nicotinic receptor M2δ peptide: a molecular dynamics simulation study. *Biophys. J.* 84:14–27.

Le Novere, N., T. Grutter, and J. P. Changeux. 2002. Models of the extracellular domain of the nicotinic receptors and of agonist- and Ca^{2+}-binding sites. *Proc. Natl. Acad. Sci. USA.* 99:3210–3215.

MacKerell, A. D., D. Bashford, M. Bellott, R. L. Dunbrack, J. D. Evanseck, M. J. Field, S. Fischer, J. Gao, H. Guo, S. Ha, D. Joseph-McCarthy, L. Kuchnir, et al. 1998. All-atom empirical potential for molecular modeling and dynamics studies of proteins. *J. Phys. Chem. B.* 102: 3586–3616.

McGehee, D. S., and L. W. Role. 1995. Physiological diversity of nicotinic acetylcholine receptors expressed by vertebrate neurons. *Annu. Rev. Physiol.* 57:521–546.

Miyazawa, A., Y. Fujiyoshi, and N. Unwin. 2003. Structure and gating mechanism of the acetylcholine receptor pore. *Nature.* 423:949–955.

Monteggia, L. M., M. Gopalakrishnan, E. Touma, K. B. Idler, N. Nash, S. P. Arneric, J. P. Sullivan, and T. Giordano. 1995. Cloning and transient expression of genes encoding the human α4 and β2 neuronal nicotinic acetylcholine receptor (nAChR) subunits. *Gene.* 155:189–193.

Noda, M., H. Takahashi, T. Tanabe, M. Toyosato, Y. Furutani, T. Hirose, M. Asai, S. Inayama, T. Miyata, and S. Numa. 1982. Primary structure of α-subunit precursor of *Torpedo californica* acetylcholine receptor deduced from cDNA sequence. *Nature.* 299:793–797.

Noda, M., H. Takahashi, T. Tanabe, M. Toyosato, S. Kikyotani, T. Hirose, M. Asai, H. Takashima, S. Inayama, T. Miyata, and S. Numa. 1983. Primary structures of β- and δ-subunit precursors of *Torpedo californica* acetylcholine receptor deduced from cDNA sequences. *Nature.* 301:251–255.

Nose, S. 1984. A unified formulation of the constant-temperature molecular-dynamics methods. *J. Chem. Phys.* 81:511–519.

Opella, S. J., F. M. Marassi, J. J. Gesell, A. P. Valente, Y. Kim, M. Oblatt-Montal, and M. Montal. 1999. Structures of the M2 channel-lining segments from nicotinic acetylcholine and NMDA receptors by NMR spectroscopy. *Nat. Struct. Biol.* 6:374–379.

Polak, E. 1971. Computational Methods in Optimization: A Unified Approach. Academic Press, New York.

Raftery, M. A., M. W. Hunkapiller, C. D. Strader, and L. E. Hood. 1980. Acetylcholine receptor: complex of homologous subunits. *Science.* 208:1454–1456.

Savage, D. F., P. F. Egea, Y. J. D. Robles-Colmenares, III, and R. M. Stroud. 2003. Architecture and selectivity in aquaporins: 2.5 Å x-ray structure of aquaporin z. *PLoS Biol.* 1:334–340.

Shrivastava, I. H., and M. S. Sansom. 2000. Simulations of ion permeation through a potassium channel: molecular dynamics of KcsA in a phospholipid bilayer. *Biophys. J.* 78:557–570.

Smart, O. S., J. M. Goodfellow, and B. A. Wallace. 1993. The pore dimensions of gramicidin A. *Biophys. J.* 65:2455–2460.

Steinlein, O. K., J. C. Mulley, P. Propping, R. H. Wallace, H. A. Phillips, G. R. Sutherland, I. E. Scheffer, and S. F. Berkovic. 1995. A missense mutation in the neuronal nicotinic acetylcholine receptor α4 subunit is associated with autosomal dominant nocturnal frontal lobe epilepsy. *Nat. Genet.* 11:201–203.

Sui, H., B. G. Han, J. K. Lee, P. Walian, and B. K. Jap. 2001. Structural basis of water-specific transport through the AQP1 water channel. *Nature.* 414:872–878.

Tang, P., P. K. Mandal, and Y. Xu. 2002. NMR structures of the second transmembrane domain of the human glycine receptor α1 subunit: model of pore architecture and channel gating. *Biophys. J.* 83:252–262.

Tang, P., and Y. Xu. 2002. Large-scale molecular dynamics simulations of general anesthetic effects on the ion channel in the fully hydrated membrane: the implication of molecular mechanisms of general anesthesia. *Proc. Natl. Acad. Sci. USA.* 99:16035–16040.

Tassonyi, E., E. Charpantier, D. Muller, L. Dumont, and D. Bertrand. 2002. The role of nicotinic acetylcholine receptors in the mechanisms of anesthesia. *Brain Res. Bull.* 57:133–150.

Thompson, J. D., D. G. Higgins, and T. J. Gibson. 1994. CLUSTAL W: improving the sensitivity of progressive multiple sequence alignment through sequence weighting, position-specific gap penalties and weight matrix choice. *Nucleic Acids Res.* 22:4673–4680.

Tieleman, D. P., and H. J. Berendsen. 1998. A molecular dynamics study of the pores formed by *Escherichia coli* OmpF porin in a fully hydrated palmitoyloleoylphosphatidylcholine bilayer. *Biophys. J.* 74:2786–2801.

Unwin, N. 2003. Structure and action of the nicotinic acetylcholine receptor explored by electron microscopy. *FEBS Lett.* 555:91–95.

Unwin, N., A. Miyazawa, J. Li, and Y. Fujiyoshi. 2002. Activation of the nicotinic acetylcholine receptor involves a switch in conformation of the α-subunits. *J. Mol. Biol.* 319:1165–1176.

White, S. H., and W. C. Wimley. 1998. Hydrophobic interactions of peptides with membrane interfaces. *Biochim. Biophys. Acta.* 1376:339–352.

Wilson, G., and A. Karlin. 2001. Acetylcholine receptor channel structure in the resting, open, and desensitized states probed with the substituted-cysteine-accessibility method. *Proc. Natl. Acad. Sci. USA.* 98:1241–1248.

Woolf, T. B., and B. Roux. 1996. Structure, energetics, and dynamics of lipid-protein interactions: a molecular dynamics study of the gramicidin A channel in a DMPC bilayer. *Proteins.* 24:92–114.

Yamakura, T., C. Borghese, and R. A. Harris. 2000. A transmembrane site determines sensitivity of neuronal nicotinic acetylcholine receptors to general anesthetics. *J. Biol. Chem.* 275:40879–40886.

Yushmanov, V. E., P. K. Mandal, Z. Liu, P. Tang, and Y. Xu. 2003a. NMR structure and backbone dynamics of the extended second transmembrane domain of the human neuronal glycine receptor α1 subunit. *Biochemistry.* 42:3989–3995.

Yushmanov, V. E., Y. Xu, and P. Tang. 2003b. NMR structure and dynamics of the second transmembrane domain of the neuronal acetylcholine receptor β2 subunit. *Biochemistry.* 42:13058–13065.

Zhou, Y., J. H. Morais-Cabral, A. Kaufman, and R. MacKinnon. 2001. Chemistry of ion coordination and hydration revealed by a K^+ channel-Fab complex at 2.0 Å resolution. *Nature.* 414:43–48.

Zubrzycki, I. Z., Y. Xu, M. Madrid, and P. Tang. 2000. Molecular dynamics simulations of a fully hydrated dimyristoylphosphatidylcholine membrane in liquid-crystalline phase. *J. Chem. Phys.* 112:3437–3441.